WHY SAM FINETUNING CAN BENEFIT OOD DETECTION? –APPENDIX–

Anonymous authors
Paper under double-blind review

A APPENDIX

A.1 THEOREM AND PROOF

We extend the convergence analysis in Mueller et al. (2023) to prove our Proposition 1.

Assumption 1. *We assume the loss function $f : R_n \to R$ to be Lipschitz continuous gradient: there exists $L > 0$ such that*

$$\|\nabla f(v) - \nabla f(w)\|_2 \leq L\|v - w\|_2, \forall v, w \in \mathbb{R}^n. \tag{1}$$

Assumption 2. *There exists $M > 0$ for any sample x_i(x_i is id data or ood data) such that*

$$\|\nabla f_{x_i}(w)\|_2^2 \leq M, \forall w \in \mathbb{R}^n. \tag{2}$$

Remark 1. *If Assumption 1 holds (L-smoothness), then any $v, w \in R_n$:*

$$|f(v) - (f(w) + \nabla f(w)^T(v - w))| \leq \frac{L}{2}\|v - w\|_2^2. \tag{3}$$

Assumption 2 guarantees that the norm of the stochastic gradient is less than the upper bound of gradient norm M. For SAM-Only-norm, the update for the norm module is:

$$\begin{aligned} w_N^{t+1/2} &= w_N^t + \rho \frac{g_{N,x_i}(w^t)}{\|g_{N,x_i}(w^t)\|} \\ w_N^{t+1} &= w_N^t - h\ g_{N,x_i}\left(w^{t+1/2}\right) \end{aligned} \tag{4}$$

The update for the other module is:

$$\begin{aligned} w_A^{t+1/2} &= w_A^t \\ w_A^{\boldsymbol{t}+1} &= w_A^t - h\ g_{A,x_i}\left(w^{t+1/2}\right). \end{aligned} \tag{5}$$

We denote the loss of the model's output as $f(w)$, the learning rate as h, the true gradient as $\nabla f(w^t)$ and the unbiased computational gradient as $g(w)$, assume that $h \leq 1/L$ then we have:

$$\begin{aligned} f(w^{t+1}) &\leq f(w^t) + \nabla f(w^t) \cdot (w^{t+1} - w^t) + \frac{L}{2}\|w^{t+1} - w^t\|^2 \\ &\leq f(w^t) - h\nabla f(w^t) \cdot g_{x_i}\left(w^{t+1/2}\right) + \frac{h^2 L}{2}\left\|g_{x_i}\left(w^{t+1/2}\right)\right\|^2 \\ &= f(w^t) - h\nabla f(w^t) \cdot g_{x_i}\left(w^{t+1/2}\right) \\ &+ \frac{h^2 L}{2}\left(\|\nabla f(w^t) - g_{x_i}(w^{t+1/2})\|^2 - \|\nabla f(w^t)\|^2 + 2\left(\nabla f(w^t) \cdot g_{x_i}(w^{t+1/2})\right)\right) \\ &= f(w^t) - \frac{Lh^2}{2}\|\nabla f(w^t)\|^2 + \frac{Lh^2}{2}\|\nabla f(w^t) - g_{x_i}(w^{t+1/2})\|^2 \\ &- (1 - Lh)h\left(\nabla f(w^t) \cdot g_{x_i}(w^{t+1/2})\right) \\ &\leq f(w^t) - \frac{Lh^2}{2}\|\nabla f(w^t)\|^2 + Lh^2\|\nabla f(w^t) - g_{x_i}(w^t)\|^2 \\ &+ Lh^2||g_{x_i}(w^t) - g_{x_i}(w^{t+1/2})||^2 - (1 - Lh)h\left(\nabla f(w^t) \cdot g_{x_i}(w^{t+1/2})\right). \end{aligned} \tag{6}$$

Take the expectation on both sides of this inequality:

$$\begin{aligned} \mathbb{E}[f(w^{t+1})] &\leq \mathbb{E}[f(w^t)] - \frac{Lh^2}{2}\mathbb{E}\|\nabla f(w^t)\|^2 + Lh^2 M \\ &+ Lh^2\|g(w^t) - g(w^{t+1/2})\|^2 - (1 - Lh)h\mathbb{E}\left[\nabla f(w^t) \cdot g(w^{t+1/2})\right]. \end{aligned} \tag{7}$$

For the penultimate term of Eq. 7, we have:

$$Lh^2\|g(w^t) - g(w^{t+1/2})\|^2 \leq L^3 h^2\|w^t - w^{t+1/2}\|^2 = L^3 h^2 \rho^2. \tag{8}$$

For the last term of Eq. 7, we have:

$$\begin{aligned} \mathbb{E}\left[\nabla f(w^t) \cdot g(w^{t+1/2})\right] &= \mathbb{E}\left[\{\nabla f_N(w^t), \nabla f_A(w^t)\} \cdot \{g_N(w^{t+1/2}), g_A(w^{t+1/2})\}\right] \\ &= \mathbb{E}[\nabla f_A(w^t) \cdot (g_A(w^{t+1/2}))] + \mathbb{E}[\nabla f_N(w^t) \cdot (g_N(w^{t+1/2}))] \\ &= \mathbb{E}[\nabla f_A(w^t) \cdot (g_A(w^{t+1/2}) - g_A(w^t) + g_A(w^t))] \\ &\quad + \mathbb{E}[\nabla f_N(w^t) \cdot (g_N(w^{t+1/2}) - g_N(w^t) + g_N(w^t))] \\ &= \mathbb{E}\left[\|\nabla f(w^t)\|^2\right] + \mathbb{E}[\nabla f_A(w^t) \cdot (g_A(w^{t+1/2}) - g_A(w^t))] \\ &\quad + \mathbb{E}[\nabla f_N(w^t) \cdot (g_N(w^{t+1/2}) - g_N(w^t))] \end{aligned} \tag{9}$$

Using $xy \leq \frac{1}{2}\|x\|_2^2 + \frac{1}{2}\|y\|_2^2$ and the Assumption 1 leads to:

$$\begin{aligned} &|\mathbb{E}[\nabla f_A(w^t) \cdot (g_A(w^{t+1/2}) - g_A(w^t))] + \mathbb{E}[\nabla f_N(w^t) \cdot (g_N(w^{t+1/2}) - g_N(w^t))]| \\ &\leq \frac{1}{2}\mathbb{E}\left[\|\nabla f(w^t)\|^2\right] + \frac{L^2}{2}\|w^{t+1/2} - w^t\|^2 = \frac{1}{2}\mathbb{E}\left[\|\nabla f(w^t)\|^2\right] + \frac{L^2\rho^2}{2} \end{aligned} \tag{10}$$

Using $h \leq 1/L$ leads to:

$$\begin{aligned} -(1 - Lh)h\mathbb{E}\left[\nabla f(w^t) \cdot g(w^{t+1/2})\right] &\leq -(1 - Lh)h\mathbb{E}\|\nabla f(w^t)\|^2 \\ &+ (1 - Lh)h\left(\frac{1}{2}\mathbb{E}\|\nabla f(w^t)\|^2 + \frac{L^2\rho^2}{2}\right) \end{aligned} \tag{11}$$

Plugging Eqs. 8 and 11 into Eq. 7 gives:

$$\begin{aligned} \mathbb{E}[f(w^{t+1})] &\leq \mathbb{E}[f(w^t)] - \frac{Lh^2}{2}\mathbb{E}\|\nabla f(w^t)\|^2 + Lh^2\|g(w^t) - g(w^{t+1/2})\|^2 \\ &- (1 - Lh)h\left(\frac{3}{2}\mathbb{E}\|\nabla f(w^t)\|^2 + \frac{L^2\rho^2}{2}\right) \\ &\leq \mathbb{E}[f(w^t)] - \frac{h}{2}\mathbb{E}\|\nabla f(w^t)\|^2 + Lh^2 M + \frac{1}{2}hL^2\rho^2(1 + Lh) \end{aligned} \tag{12}$$

Usually, we use the cross-entroy loss in multi-classification tasks. $f(w^t)$ can be thus re-written as:

$$f(w^t) = f(g(w^t)) = -log\frac{e^{max(g_i)}}{\sum\limits_{i=1}^{n} e^{g_i}} = -max(g_i) + log\sum_{i=1}^{n} e^{g_i} \tag{13}$$

where $g(w^t) = [g_1, g_2, ..., g_n]$ denotes the logit output of the model, n is the total number of classes in the classification task. Thus, Eq. 12 can be rewritten as the following inequality:

$$\triangle(-max(g_i) + log\sum_{i=1}^{n} e^{g_i}) \leq -\frac{h}{2}\mathbb{E}\|\nabla f(w^t)\|^2 + Lh^2M + \frac{1}{2}hL^2\rho^2(1 + Lh) \tag{14}$$

We notice that $log \sum\limits_{i=1}^{n} e^{g_i}$ takes the same form of enengy score (Liu et al., 2020). Then, we can get the upper bound of the score change.

$$\triangle(\text{Energy Score}) \leq -\frac{h}{2}\mathbb{E}\|\nabla f(w^t)\|^2 + \triangle(max(g_i)) + Lh^2M + \frac{1}{2}hL^2\rho^2(1 + Lh) \tag{15}$$

A.2 Additional Visualizations.

Pseudo-OOD data. Fig. 1 and 2 visualize the exemplary pseudo-OOD data generated from ID data. The pseudo-OOD data can mimic the real-world OOD data and improve the detection performance.

Original ID data | *Jigsaw Puzzle* | *Jigsaw Puzzle+Invert*

Figure 1: Visualization of pseudo OOD data on ImageNet-1K (Deng et al., 2009).

Original ID data | *Jigsaw Puzzle* | *Jigsaw Puzzle+Invert*

Figure 2: Visualization of pseudo OOD data on CIFAR-10 (Krizhevsky et al., 2009).

Score distributions of ResNetv2-101. Fig. 3 and 4 displays the score distributions of `MSP` and `RankFeat` with ResNetv2-101. Our `SFT` greatly reduces the overlapping of ID and OOD scores, enhancing the OOD detection performance.

Score distributions of T2T-ViT-24. Fig. 5, 6, and 7 depicts the score distributions of `MSP`, `Energy` and `RankFeat` with T2T-ViT-24, respectively. Empowered by our fine-tuning, the performance of baseline methods is greatly boosted to better distinguish OOD samples.

Gradient norm and maximum output logit distributions of ResNetv2-101 on the other OOD testsets. Fig. 8, 9 and 10 display the gradient norm of FC layer and maximum output logit distributions on iNaturalist, SUN and Places OOD testsets with ResNetv2-101. The observation from the above figures meets our previous theoretical analysis on the working mechanism of `SFT`.

Gradient norm and maximum output logit distributions of T2T-ViT-24. Fig. 11, 12, 13 and 14 display the gradient norm of FC layer and maximum output logit distributions on iNaturalist, SUN, Places and Textures OOD testsets with T2T-ViT-24, respectively. The observation from the above figures meets our previous theoretical analysis on the working mechanism of `SFT`: we reduce the upper bound of score change by reducing the maximum logit output.

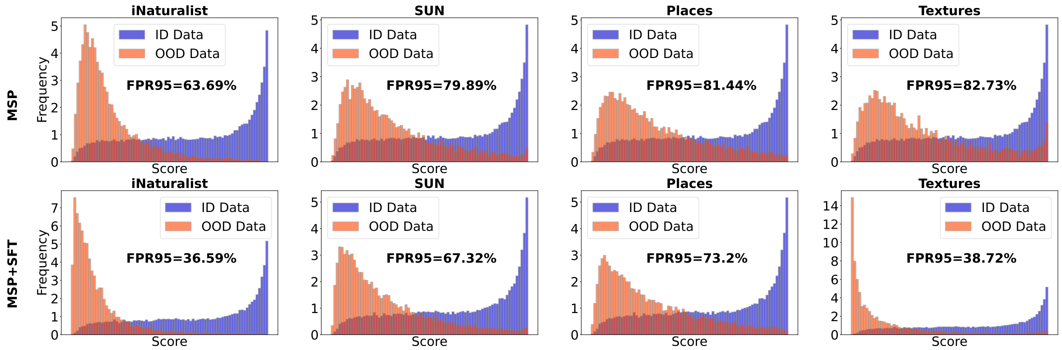

Figure 3: Score distributions of `MSP` with ResNetv2-101.

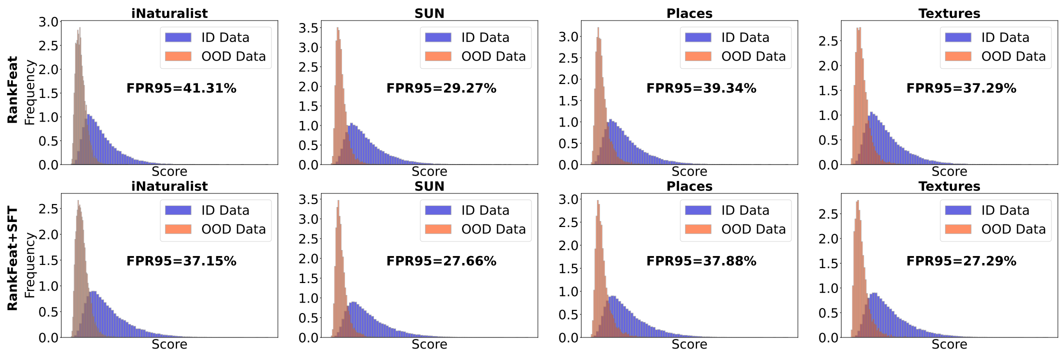

Figure 4: Score distributions of `RankFeat` with ResNetv2-101.

REFERENCES

Jia Deng, Wei Dong, Richard Socher, Li-Jia Li, Kai Li, and Li Fei-Fei. Imagenet: A large-scale hierarchical image database. In *CVPR*, pp. 248–255. Ieee, 2009.

Alex Krizhevsky, Geoffrey Hinton, et al. Learning multiple layers of features from tiny images. 2009.

Weitang Liu, Xiaoyun Wang, John Owens, and Yixuan Li. Energy-based out-of-distribution detection. *NeurIPS*, 33:21464–21475, 2020.

Maximilian Mueller, Tiffany Vlaar, David Rolnick, and Matthias Hein. Normalization layers are all that sharpness-aware minimization needs. *arXiv preprint arXiv:2306.04226*, 2023.

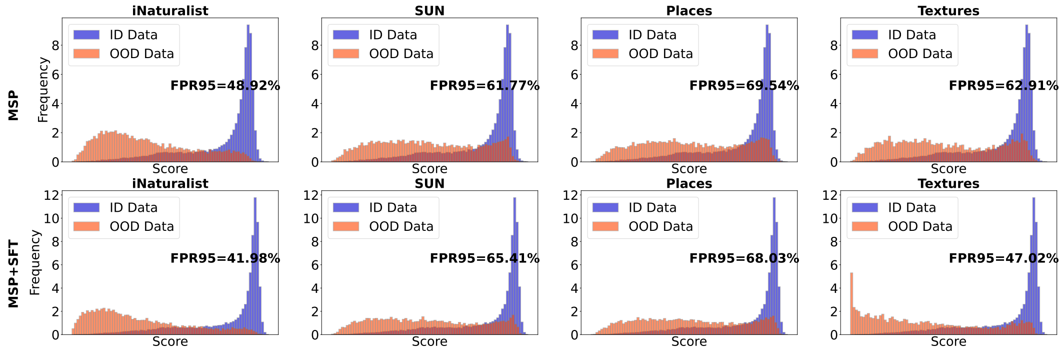

Figure 5: Score distributions of `MSP` with T2T-ViT-24.

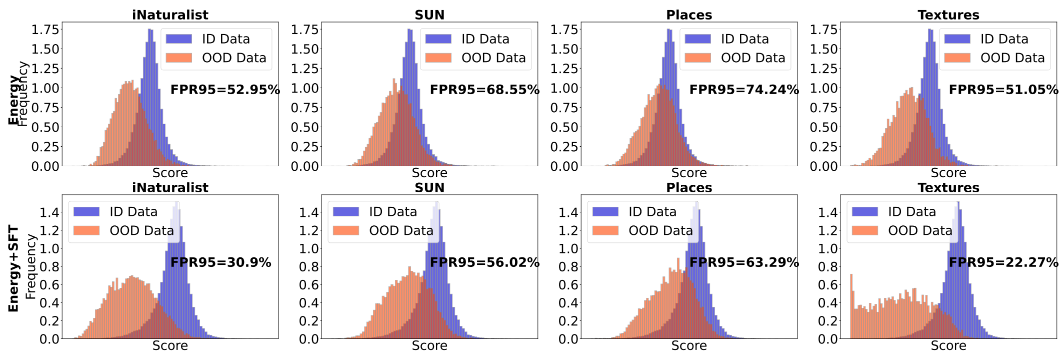

Figure 6: Score distributions of `Energy` with T2T-ViT-24.

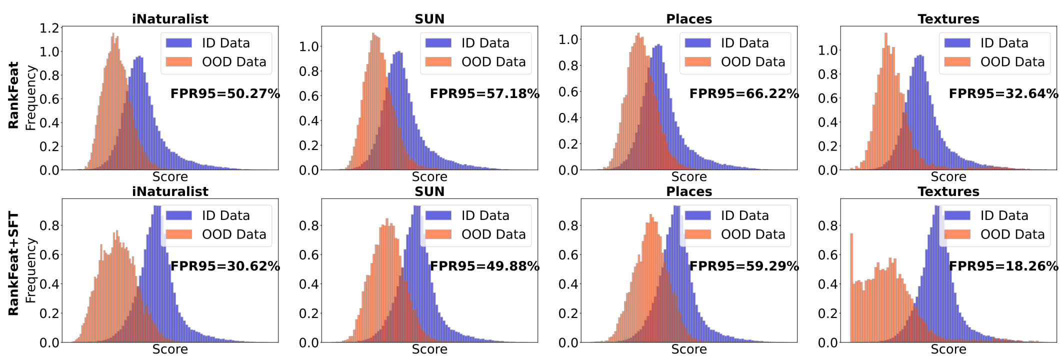

Figure 7: Score distributions of `RankFeat` with T2T-ViT-24.

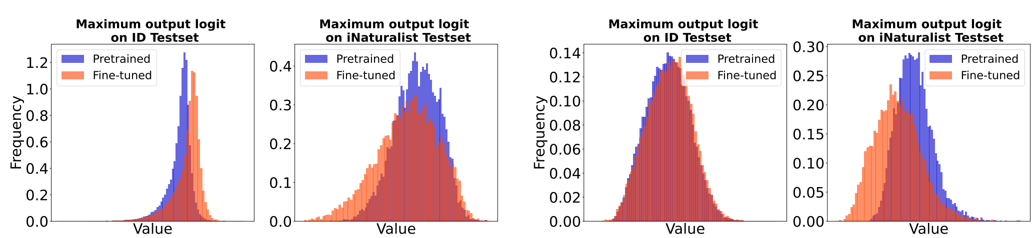

(a) gradient norm of FC layer (b) maximum output logit of model

Figure 8: The gradient norm of FC layer and maximum output logit of model on ID and **iNaturalist** OOD testset with ResNetv2-101.

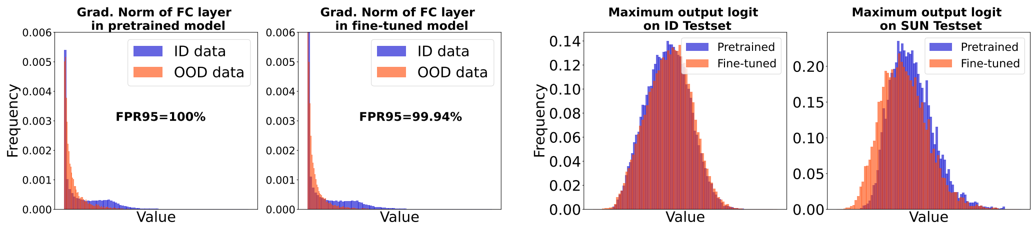

(a) gradient norm of FC layer (b) maximum output logit of model

Figure 9: The gradient norm of FC layer and maximum output logit of model on ID and **SUN** OOD testset with ResNetv2-101.

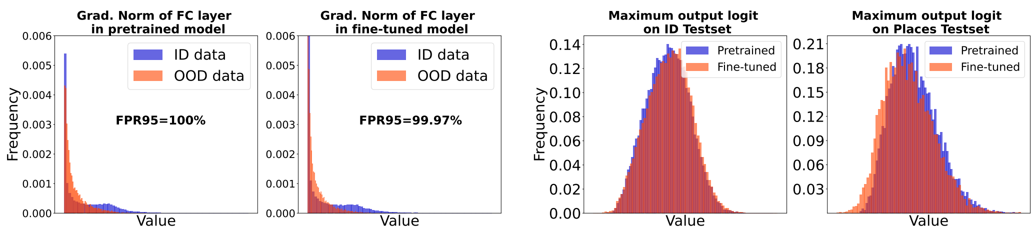

(a) gradient norm of FC layer (b) maximum output logit of model

Figure 10: The gradient norm of FC layer and maximum output logit of the model on ID and **Places** OOD testset with ResNetv2-101.

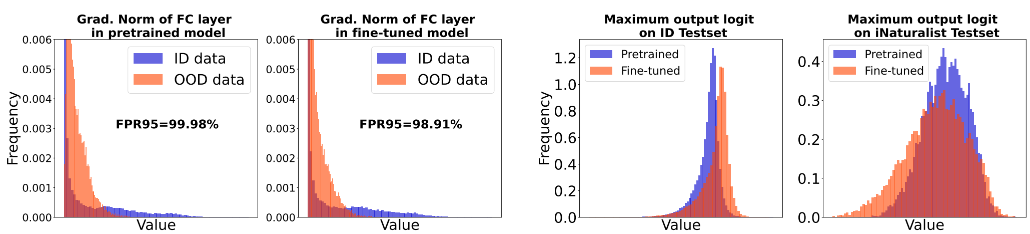

(a) gradient norm of FC layer (b) maximum output logit of model

Figure 11: The gradient norm of FC layer and maximum output logit of model on ID and **iNaturalist** OOD testset with T2T-ViT-24.

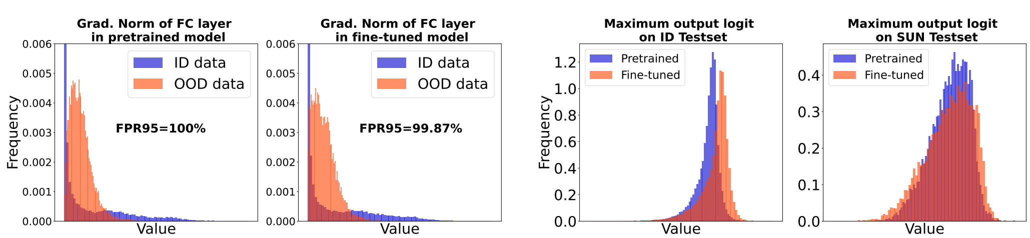

(a) gradient norm of FC layer (b) maximum output logit of model

Figure 12: The gradient norm of FC layer and maximum output logit of model on ID and **SUN** OOD testset with T2T-ViT-24.

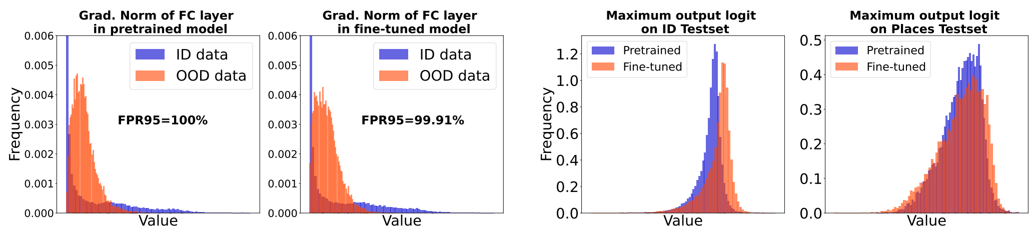

(a) gradient norm of FC layer (b) maximum output logit of model

Figure 13: The gradient norm of FC layer and maximum output logit of model on ID and **Places** OOD testset with T2T-ViT-24.

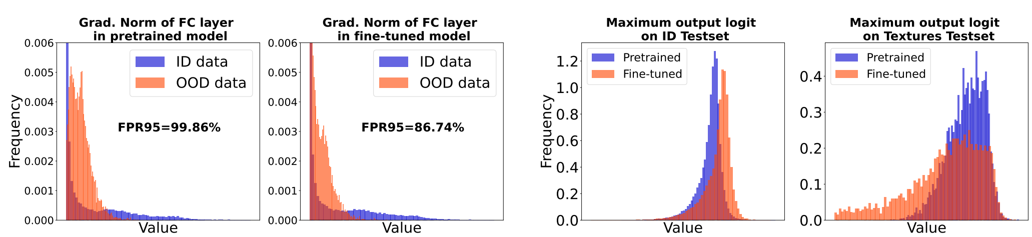

(a) gradient norm of FC layer (b) maximum output logit of model

Figure 14: The gradient norm of FC layer and maximum output logit of model on ID and **Textures** OOD testset with T2T-ViT-24.